J. Fluid Mech. (2022), *vol*. 942, A19, doi:10.1017/jfm.2022.373

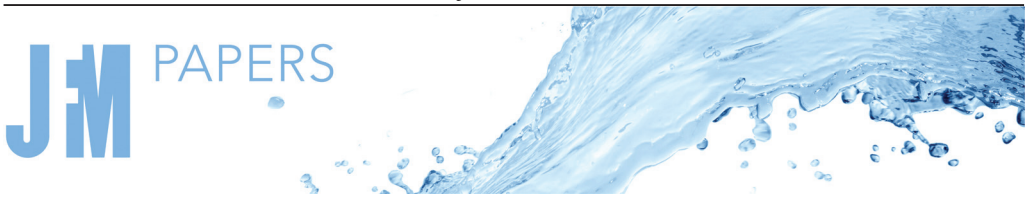

Bolgiano–Obukhov scaling in two-dimensional isotropic convection

Jin-Han Xie[1,2] **and Shi-Di Huang**[3,4]

[1]Department of Mechanics and Engineering Science at College of Engineering, and State Key Laboratory for Turbulence and Complex Systems, Peking University, Beijing 100871, PR China

[2]Joint Laboratory of Marine Hydrodynamics and Ocean Engineering, Pilot National Laboratory for Marine Science and Technology (Qingdao), Shandong 266237, PR China

[3]Department of Mechanics and Aerospace Engineering and Center for Complex Flows and Soft Matter Research, Southern University of Science and Technology, Shenzhen 518055, PR China

[4]Guangdong Provincial Key Laboratory of Turbulence Research and Applications, Department of Mechanics and Aerospace Engineering, Southern University of Science and Technology, Shenzhen 518055, PR China

(Received 12 October 2021; revised 13 March 2022; accepted 21 April 2022)

The existence of Bolgiano–Obukhov (BO) scaling in Rayleigh–Bénard convection (RBC) has long been speculated. However, due to the inhomogeneity and anisotropy of the flow, and the lack of clear scale separation, no conclusive evidence has been found. To avoid these non-ideal factors, we construct an idealized isotropic convection system by introducing an additional horizontal buoyancy field to RBC in a doubly periodic domain. We focus on the two-dimensional case so that its upscale kinetic energy flux can enable a long inertial range for detecting the BO scaling. Through direct numerical simulations of this system, we justify the existence of BO scaling using second- and third-order structure functions, which are in good agreement with our theoretically obtained scaling relations from the Kármán–Howarth–Monin equations. These theoretical and numerical results provide direct support for the conjecture that the existence of the BO scaling in RBC is associated with the inverse kinetic energy cascade. For higher-order structure functions, we found strong intermittent effects in the buoyancy field, but not in the velocity. By comparing the present system with the canonical anisotropic RBC in a periodic domain, the effects of anisotropy on the scaling properties are elucidated.

Key words: homogeneous turbulence, isotropic turbulence, turbulent convection

1. Introduction

Thermal convection is important for nature and engineering applications. An idealized system to study thermal convection is Rayleigh–Bénard convection (RBC), where a fluid

layer is heated from below and cooled from above. Despite tremendous progress achieved in the understanding of RBC over the years (Ahlers, Grossmann & Lohse 2009; Lohse & Xia 2010; Chillà & Schumacher 2012; Xia 2013; Verma, Kumar & Pandey 2017), there remain several major issues that are not settled fully. One of them is the existence of the so-called Bolgiano–Obukhov (BO) scaling.

As a generalization to the structure function theory for isotropic turbulence (Monin & Yaglom 1975; Frisch 1995), the BO theory was proposed initially for density stratified turbulence (Bolgiano 1959; Obukhov 1959). In the BO scenario, the nth-order structure functions for the velocity and temperature fields can be expressed as (with intermittency ignored)

$$S_n^u(r) = \overline{\delta u^n} \sim r^{3n/5} \quad \text{and} \quad S_n^\theta(r) = \overline{\delta\theta^n} \sim r^{n/5}, \tag{1.1a,b}$$

where δu and $\delta\theta$ are the velocity and temperature increments with a separation r, respectively. These scaling relations are distinctive from those based on the celebrated Kolmogorov–Obukhov (KO) theory (Kolmogorov 1941; Obukhov 1949), in which the scaling exponents in the non-intermittent case are equal to $n/3$ for both velocity and temperature structure functions.

Although the BO scaling was developed originally for stably stratified turbulence, the experimental work on temperature power spectra in turbulent RBC by Wu *et al.* (1990) led to some theoretical arguments that the BO scaling can also be observed in unstably stratified convective turbulence (L'vov 1991; Yakhot 1992). Since then, numerous efforts have been devoted to the search for the BO scaling in turbulent RBC, but its existence is still debatable (for review, see Lohse & Xia 2010). According to the most recent understandings (Lohse & Xia 2010; Ching 2014; Kunnen & Clercx 2014), there are several factors that prevent the observation of the BO scaling in a canonical RBC system. (*a*) The impact of the wall makes the convection inhomogeneous, so the statistics of velocity and temperature are different in different locations of the convection system (Camussi & Verzicco 2004; Sun, Zhou & Xia 2006; Li *et al.* 2021*a*,*b*). (*b*) The turbulent flow is anisotropic, which in part is also caused by the wall. More intrinsically, RBC is driven by buoyancy along the vertical direction, while the buoyancy effect in the horizontal direction is absent. Even though the bulk flow at the centre of RBC has been found to be isotropic (Zhou, Sun & Xia 2008; Ni, Huang & Xia 2011), no buoyancy effect is manifested in that region. (*c*) There exist large-scale circulations in wall-bounded systems, which modify the turbulent dynamics and thus contaminate the small-scale statistics (Kunnen *et al.* 2008; Li *et al.* 2021*b*). To disentangle the mixed flow dynamics, one should decompose the perturbation and mean flow (Mashiko *et al.* 2004) or analyse the data via conditional statistics (Ching 2007; Ching *et al.* 2013). (*d*) The last factor is the almost impossibility of fulfilling the condition of scale separation that gives the distinct inertial range of BO cascade scenario (Grossmann & Lohse 1991, 1992). Thanks to detailed numerical studies (Kunnen *et al.* 2008; Kaczorowski & Xia 2013; Kaczorowski, Chong & Xia 2014; Kunnen & Clercx 2014), this fundamental obstacle has become more evident in the past decade.

To avoid the impact of the walls, which contribute to the first three complicating factors mentioned above, some approaches have been proposed to explore the BO scaling in RBC under more ideal conditions. For example, Calzavarini, Toschi & Tripiccione (2002) employed a lattice Boltzmann scheme to simulate RBC directly with the lateral boundaries being periodic and the top/bottom boundaries being stress-free. These numerical settings allow us to maintain the flow homogeneity along horizontal directions, and reduce the effects of viscous shear near the walls. However, due to the limited resolution of their simulations, no evident scaling range can be detected in the structure functions. Instead, they resorted to the extended self-similarity analysis (Benzi *et al.* 1993) to test the

BO phenomenology indirectly. Moreover, although Calzavarini *et al.* (2002) found a BO-like scaling near the top/bottom walls, they cannot distinguish the effects of buoyancy and viscous shear, as the stress-free boundary condition does not suppress the viscous boundary layers completely. Thus they suggested that it is helpful to perform simulations with periodic boundary conditions in all directions, i.e. homogeneous RBC (Lohse & Toschi 2003).

This sort of homogeneous convection system was first investigated by Borue & Orszag (1997), who adopted hyperviscosity to eliminate the unpleasant 'elevator modes' (Calzavarini *et al.* 2006). Through simulating RBC computationally in a triply periodic box driven by a constant vertical temperature gradient, Borue & Orszag (1997) found that the scaling laws of the second-order correlation functions favour the KO picture rather than the BO one. The most important reason for the absence of the BO scaling in homogeneous RBC is that the Bolgiano scale, only above which the buoyancy becomes dominant and thus the BO scaling is expected to hold, is of the order of the system size (Borue & Orszag 1997; Biferale *et al.* 2003). The lack of a wide separation of length scales (i.e. factor (d) aforementioned), which is also valid for canonical RBC and horizontally periodic RBC, seems to imply that detecting the BO scaling in RBC is unrealistic.

The situations discussed above are based on RBC in three dimensions. To obtain a wide inertial range for the BO scaling, a two-dimensional (2-D) configuration may be considered by taking advantage of its intrinsic feature of inverse kinetic energy cascade (Kraichnan 1967). This phenomenology was first considered by Chertkov (2003) in the study of another kind of buoyancy-driven turbulent flows, namely the Rayleigh–Taylor (RT) turbulence (see Boffetta & Mazzino (2017) and Zhou (2017) for reviews of this subject). According to Chertkov (2003), while the three-dimensional (3-D) RT turbulence follows the KO picture, the BO scaling can be expected for the 2-D case. These predictions have been confirmed numerically and extended to the cases with intermittency effects (Celani, Mazzino & Vozella 2006; Boffetta *et al.* 2009; Zhou 2013). The relation between the scaling properties in 3-D and 2-D RT systems is revealed further by the study in the quasi-2-D case. By using a configuration with strong confinement in one horizontal direction, Boffetta *et al.* (2012) observed the coexistence of KO and BO scaling regimes separated by the Bolgiano scale. In particular, due to the geometrical constraint, the flow at scales larger than the Bolgiano scale behaves like 2-D turbulence. This interesting finding brought about a conjecture that the BO phenomenology could be observed whenever an upscale energy transfer is induced in the turbulent flow, but its validation in RBC has not been checked as far as we know.

As RT turbulence and homogeneous RBC, both being free of physical boundaries, are dynamically similar (Mazzino 2017), one would expect that the phenomenological model for RT turbulence is equally applicable to homogeneous RBC. Indeed, the realization of the BO scaling in 2-D homogeneous RBC has been confirmed numerically for lower-order structure functions (Celani, Mazzino & Vergassola 2001; Celani *et al.* 2002). It is further found in these studies that the velocity structure functions at higher orders still closely follow the BO prediction, but the temperature ones show strongly intermittent effects, which is in line with the observations in quasi-equilibrium RT turbulence (Celani *et al.* 2006). In a similar numerical study by Biskamp, Hallatschek & Schwarz (2001), which investigated the scaling properties of 2-D homogeneous RBC less directly, the BO scaling is also found to be approximately valid, though their previous work using a lower numerical resolution precluded the BO scaling even for the second-order structure functions (Biskamp & Schwarz 1997). Note that all these studies were limited to the statistics of isotropic structure functions (Mazzino 2017). Thus there remains a question

of whether the isotropic and anisotropic structure functions are independent. If not, then there should be an impact of anisotropy on the scaling properties, making the latter differ from the predictions of the isotropic theory.

The simulations in 2-D RBC have stimulated some innovative 2-D convection experiments using soap films/bubbles driven by a temperature gradient (Zhang & Wu 2005; Zhang, Wu & Xia 2005; Seychelles *et al.* 2008, 2010). These experiments also observed a BO-like scaling when the temperature gradient is large enough (Zhang & Wu 2005; Seychelles *et al.* 2010). However, while the probability density functions (p.d.f.s) of the velocity increment in these studies show exponential tails that manifest intermittent effects, the p.d.f.s of the temperature increment are nearly Gaussian (i.e. non-intermittent), which contradicts the observation in the simulations of 2-D homogeneous RBC (Biskamp *et al.* 2001; Celani *et al.* 2001). Although the reason for this discrepancy remains unknown, it is clear that the flow fields in these convection experiments are neither homogeneous nor isotropic (Zhang *et al.* 2005; Seychelles *et al.* 2008), and only horizontal velocity structure functions were examined in the study by Seychelles *et al.* (2010). These complicating factors will undoubtedly affect the scaling properties, as we discussed at the beginning of this Introduction.

The motivation of this paper is to explore the BO scaling in a situation where all the non-ideal conditions are absent. This requires us to avoid the impact of inhomogeneity, anisotropy and large-scale circulations, and to generate a long inertial range for energy cascade. Therefore, we constructed an isotropic convection system by introducing a horizontal buoyancy field to RBC in a 2-D periodic domain. This isotropic system will be introduced in § 2, followed by a theoretical argument on the BO scenario and the accordingly obtained expressions of statistical quantities in § 3. Then we will perform numerical simulations in § 4 to justify the isotropy of the system and examine the corresponding statistical quantities. These results will be compared with those obtained in the canonical anisotropic RBC. Finally, we summarize and discuss our findings in § 5. Appendix A presents the structure functions of some non-traditional quantities brought about by the presence of the newly introduced horizontal buoyancy field.

2. Formulation

We start from the 2-D RBC with the governing equations

$$\nabla^2\psi_t + \mathcal{J}(\psi, \nabla^2\psi) - g\beta\theta_x = \nu_0\nabla^4\psi, \tag{2.1a}$$

$$\theta_t + \mathcal{J}(\psi, \theta) - \bar{\theta}_z\psi_x = \kappa_0\nabla^2\theta, \tag{2.1b}$$

where ψ is the streamfunction such that $(u, w) = (-\partial_z\psi, \partial_x\psi)$, g is gravity, β is the expansion coefficient, θ is the temperature, $\bar{\theta}_z$ is the background temperature stratification that leads to linear instability, and ν_0 and κ_0 are viscosity and thermal diffusivity, respectively.

The governing equations above are inherently anisotropic, which brings about complications to justify the isotropic theory of BO. In addition, simulations of RBC in a doubly periodic domain will generate elevator modes that modify drastically the statistically steady states (Calzavarini *et al.* 2006). To prevent these effects, we construct an isotropic convection system by adding an additional buoyancy component subjected to

a 'horizontal gravity':

$$\nabla^2\psi_t + \mathcal{J}(\psi, \nabla^2\psi) - g\beta\theta_x + g\beta\sigma_z = \nu_0\,\nabla^4\psi, \tag{2.2a}$$

$$\sigma_t + \mathcal{J}\,(\psi, \sigma) + \bar{\sigma}_x\psi_z = \kappa_0\,\nabla^2\sigma, \tag{2.2b}$$

$$\theta_t + \mathcal{J}\,(\psi, \theta) - \bar{\theta}_z\psi_x = \kappa_0\,\nabla^2\theta. \tag{2.2c}$$

Here, σ is the new horizontal buoyancy. To ensure the isotropy of the system, we further set the background gradients to be $\bar{\theta}_z = \bar{\sigma}_x$, and the diffusivity of the two buoyancy fields are also taken to be the same.

As we focus on the inertial range dynamics in statistically steady states, to extend the inertial range with fixed resolutions, we replace the normal viscosity (diffusivity) with the hyperviscosity (hyperdiffusivity), and introduce the hypoviscosity and hypodiffusivity to absorb the upscale energy flux (cf. Celani *et al.* 2002). Thus (2.2*a*)–(2.2*c*) become

$$\nabla^2\psi_t + \mathcal{J}(\psi, \nabla^2\psi) - g\beta\theta_x + g\beta\sigma_z = \nu^*\,\nabla^8\psi + \alpha^*\psi, \tag{2.3a}$$

$$\sigma_t + \mathcal{J}\,(\psi, \sigma) + \bar{\sigma}_x\psi_z = \kappa^*\,\nabla^6\sigma + \mu^*\Delta^{-1}\sigma, \tag{2.3b}$$

$$\theta_t + \mathcal{J}\,(\psi, \theta) - \bar{\theta}_z\psi_x = \kappa^*\,\nabla^6\theta + \mu^*\Delta^{-1}\theta. \tag{2.3c}$$

Through introducing the non-dimensionalization

$$t \to \frac{1}{\sqrt{g\beta\bar{\theta}_z}}\,t, \quad \boldsymbol{x} \to L\boldsymbol{x}, \quad \psi \to \sqrt{g\beta\bar{\theta}_z}\,L^2\psi \quad \text{and} \quad (\theta, \sigma) \to \bar{\theta}_z L(\theta, \sigma), \tag{2.4a–d}$$

where L is a characteristic length of the domain size, (2.3*a*)–(2.3*c*) become

$$\nabla^2\psi_t + \mathcal{J}\left(\psi, \nabla^2\psi\right) - \theta_x + \sigma_z = \nu\,\nabla^8\psi + \alpha\psi, \tag{2.5a}$$

$$\sigma_t + \mathcal{J}\,(\psi, \sigma) + \psi_z = \kappa\,\nabla^6\sigma + \mu\Delta^{-1}\sigma, \tag{2.5b}$$

$$\theta_t + \mathcal{J}\,(\psi, \theta) - \psi_x = \kappa\,\nabla^6\theta + \mu\Delta^{-1}\theta, \tag{2.5c}$$

with

$$\nu = \frac{\nu^*}{L^6\sqrt{g\beta\bar{\theta}_z}}, \quad \kappa = \frac{\kappa^*}{L^6\sqrt{g\beta\bar{\theta}_z}}, \quad \alpha = \frac{\alpha^*L^2}{\sqrt{g\beta\bar{\theta}_z}} \quad \text{and} \quad \mu = \frac{\mu^*L^2}{\sqrt{g\beta\bar{\theta}_z}}. \tag{2.6a–d}$$

These non-dimensional parameters can be linked to the oft-used control parameters of canonical RBC, namely the Rayleigh (Ra) and Prandtl (Pr) numbers, through the definitions

$$Ra = \frac{1}{\nu\kappa} = \frac{g\beta\bar{\theta}_z L^{12}}{\nu^*\kappa^*} \quad \text{and} \quad Pr = \frac{\kappa}{\nu} = \frac{\kappa^*}{\nu^*}. \tag{2.7a,b}$$

Here, the definition of Pr shares the same form as the usual definition, except that ν^* and κ^* are hyperviscosity and hyperdiffusivity, respectively.

It is noteworthy that because of the hyperviscosity and hyperdiffusivity used, we may not compare directly the above-defined Ra with the oft-used one based on normal viscosity and diffusivity. Nevertheless, for curiosity and also a better understanding of the present isotropic system, we can consider a virtual canonical RBC where the dissipation scale and the potential energy dissipation rate are the same as those in the system given by (2.5*a*)–(2.5*c*). For this virtual system, the normal diffusivity can be expressed as $\mu_{virtual} \sim$

$\mu^{1/4}\epsilon_P^{1/4}$, with ϵ_P being the small-scale potential energy dissipation rate. Then, with other quantities fixed, the corresponding Ra in the virtual system scales as $Ra_{virtual} \sim Ra^{1/4}$. In other words, a value $Ra = 10^{32}$ based on the present definition is equivalent to an order of 10^8 in the usual case.

With the above construction, we obtain an isotropic system described by (2.5*a*)–(2.5*c*). If we rotate the x- and z-coordinates by an angle γ via the transformation

$$x' = x\cos\gamma - z\sin\gamma \quad \text{and} \quad z' = x\sin\gamma + z\cos\gamma, \tag{2.8a,b}$$

introduce

$$\psi'(x', z') = \psi(x, z), \tag{2.9}$$

and define new scalars

$$\sigma' = \sigma\cos\gamma - \theta\sin\gamma \quad \text{and} \quad \theta' = \sigma\sin\gamma + \theta\cos\gamma, \tag{2.10a,b}$$

then this system is invariant. Note that this isotropic convection system resembles the isotropic inertia-gravity-wave system studied by Xie & Bühler (2019*b*), which consists of two stably stratified buoyancy fields.

For a single Fourier mode, $\exp(\lambda t - 1\mathrm{i}(kx + mz))$, the linear growth rate λ with respect to the zero state of (2.5*a*)–(2.5*c*) is

$$\lambda = \frac{1}{2}\left(-(\nu+\kappa)K^6 - (\alpha+\mu)K^{-2} + \sqrt{4 + \left[(\nu-\kappa)K^6 + (\alpha-\mu)K^{-2}\right]^2}\right), \tag{2.11}$$

where $K = \sqrt{k^2 + m^2}$, with k and m the horizontal and vertical wavenumbers, respectively. The linear growth rate inherits the isotropy of system governed by (2.2*a*)–(2.2*c*), which differs from the canonical RBC system described by (2.1*a*)–(2.1*b*) that has an anisotropic linear growth rate.

3. Theoretical argument for the existence of BO scaling

Since the system described by (2.5*a*)–(2.5*c*) is isotropic, and if we consider the situation with no external forcing, it will develop into a statistically homogeneous isotropic steady state, which is the focus of the present paper. We can explore the statistical properties using two-point structure functions.

3.1. *Derivation of the Kármán–Howarth–Monin equations*

Consider two measured points located at $\boldsymbol{x}$ and $\boldsymbol{x}' = \boldsymbol{x} + \boldsymbol{r}$, where $\boldsymbol{r}$ is the displacement of these two points. We denote the quantities evaluated at $\boldsymbol{x}'$ with a prime, e.g. $u' = u(\boldsymbol{x}') = u(\boldsymbol{x} + \boldsymbol{r})$. Homogeneity implies that for two-point statistical quantities, the spatial derivatives follow

$$\boldsymbol{\nabla} = -\boldsymbol{\nabla}' = -\boldsymbol{\nabla}_{\boldsymbol{r}}, \tag{3.1}$$

where $\boldsymbol{\nabla}'$ and $\boldsymbol{\nabla}_{\boldsymbol{r}}$ denote the gradients taken with respect to $\boldsymbol{x}'$ and $\boldsymbol{r}$, respectively.

For statistically steady states, by multiplying ψ', σ' and θ' to (2.5*a*), (2.5*b*) and (2.5*c*), and then adding the corresponding conjugate equations, respectively, we obtain

the Kármán–Howarth–Monin (KHM) equations (cf. Monin & Yaglom 1975; Frisch 1995) for (2.5*a*)–(2.5*c*):

$$-\frac{1}{2}\boldsymbol{\nabla}\cdot\overline{\delta\boldsymbol{u}\left(\delta u^2+\delta w^2\right)}+\left(\overline{u\sigma'}+\overline{u'\sigma}-\overline{w\theta'}-\overline{w'\theta}\right)=D_\psi, \tag{3.2a}$$

$$-\frac{1}{2}\boldsymbol{\nabla}\cdot\overline{\delta\boldsymbol{u}\,\delta\sigma^2}+\left(\overline{u\sigma'}+\overline{u'\sigma}\right)=D_\sigma, \tag{3.2b}$$

$$-\frac{1}{2}\boldsymbol{\nabla}\cdot\overline{\delta\boldsymbol{u}\,\delta\theta^2}-\left(\overline{w\theta'}+\overline{w'\theta}\right)=D_\theta, \tag{3.2c}$$

where

$$D_\psi=-2\nu\,\overline{\nabla^4\psi\,\nabla'^4\psi'}-2\alpha\overline{\psi\psi'}, \tag{3.3a}$$

$$D_\sigma=-2\kappa\,\overline{\nabla^3\sigma\,\nabla'^3\sigma'}-2\mu\overline{\Delta^{1/2}\sigma\,\Delta'^{1/2}\sigma'}, \tag{3.3b}$$

$$D_\theta=-2\kappa\,\overline{\nabla^3\theta\,\nabla'^3\theta'}-2\mu\overline{\Delta^{1/2}\theta\,\Delta'^{1/2}\theta'}, \tag{3.3c}$$

are the effects of dissipation and diffusivity. Note that $D_\psi|_{r=\mathbf{0}}$, $D_\sigma|_{r=\mathbf{0}}$ and $D_\theta|_{r=\mathbf{0}}$ are all negative.

For the present isotropic convection system, we know qualitatively that the instability brings about energy injection through the buoyancy terms, i.e. the quadratic terms on the left-hand sides of (3.2*a*)–(3.2*c*), then the nonlinear advection transfers energy across scales, and finally, the energy is dissipated due to dissipation and diffusivity. Since an important feature of the BO theory is the interaction between the potential energy and kinetic energy, this physical picture inspires us to argue the BO scaling from the energy transfer processes.

3.2. *Argument based on energy flux*

Taking the Fourier transform of the KHM equations (3.2*a*)–(3.2*c*), we obtain the spectral energy equation, which can be written symbolically as

$$\partial_K F_K+B=D_K, \tag{3.4a}$$

$$\partial_K F_P+B=D_P, \tag{3.4b}$$

where F is the energy flux across scales, B is the buoyancy effect that injects energy into the system, D is the dissipation, and the subindices K and P denote the kinetic and potential energy, respectively.

We now argue the existence of BO scaling based on the transfer directions of the kinetic and potential energy. To be specific, we assume that for the present 2-D isotropic system, the kinetic energy transfers upscale, while the potential energy transfers downscale. This assumption is based on the 2-D turbulence's upscale energy transfer (Kraichnan 1967) and the forward cascade of temperature field in a turbulent velocity field (Obukhov 1949; Corrsin 1951). Although in some cases, the existence of potential parts may lead to a downscale flux of the kinetic energy in two dimensions (Xie & Bühler 2019*b*), in § 4 we will demonstrate numerically the validity of this assumption for the present system.

The potential energy transfers downscale, so if the buoyancy generation is a power function of wavenumber (i.e. a simple cascade picture), say $B\sim K^{-a}$ ($a>1$), then the

potential energy flux can be expressed as

$$F_P \propto \int_{K_0}^{K} \tilde{K}^{-a}\,\mathrm{d}\tilde{K} = K_0^{-a+1} - K^{-a+1}, \tag{3.5}$$

where K_0 is the large-scale dissipation wavenumber. This formula immediately implies that a constant potential energy flux is seen at small scales when $K/K_0 \gg 1$. We can also obtain the relative importance of the constant flux and the energy injection by comparing F_P and $K\,\partial_K F_P$:

$$\left|\frac{F_P}{K\,\partial_K F_P}\right| = \frac{1}{a-1}\left(\left(\frac{K_0}{K}\right)^{1-a} - 1\right), \tag{3.6}$$

which tends to infinity, implying that the flux is dominant as $K \to \infty$. Therefore, the BO scaling induced by constant potential energy flux should be observed at small scales.

For the kinetic energy, which transfers upscale, we have

$$F_K \propto \int_{-\infty}^{K} \tilde{K}^{-a}\,\mathrm{d}\tilde{K} = -\frac{1}{1-a}\,K^{-a+1}. \tag{3.7}$$

Note that because of the opposite directions of energy transfer, the integration directions in (3.7) and (3.5) are opposite. Similarly, we have

$$\left|\frac{F_K}{K\,\partial_K F_K}\right| = \frac{1}{a-1}, \tag{3.8}$$

implying a balance between the transfer and injection of kinetic energy, which completes the BO scenario.

It is noteworthy that because of the inverse cascade of kinetic energy, the Bolgiano scale is not important in the 2-D case. To be specific, we can estimate the Bolgiano scale using the expression (cf. Lohse & Xia 2010)

$$l_B = \epsilon_K^{5/4}\epsilon_P^{-3/4}(\beta g)^{-3/2}, \tag{3.9}$$

where ϵ_K and ϵ_P are the small-scale kinetic and potential energy dissipation rates, respectively. Because ϵ_K is approximately zero as the downscale energy flux is negligibly small in 2-D turbulence, we have $l_B = 0$ theoretically, which in numerical simulations is approximately equal to the smallest resolved length scale (Celani *et al.* 2002). The negligibly small l_B also implies the non-existence of the KO scaling in the present 2-D system.

3.3. *Scalings of structure functions*

From the perspective of the KHM equations (3.2*a*)–(3.2*c*), the BO scaling is consistent with the knowledge of 2-D and 3-D turbulence, which transfers energy upscale and downscale, respectively. The key is the link between the direction of energy flux and the anomaly's influence on the procedure of obtaining the expressions for the third-order structure functions. Specifically, in 3-D turbulence, where the kinetic energy transfers downscale and dissipates, we can ignore the effect of energy injection, and take the leading-order approximation of the dissipation as the energy dissipation in the KHM equations to obtain the Kolmogorov 4/5-law (Kolmogorov 1941; Frisch 1995). While for 2-D turbulence, where the kinetic energy transfers upscale, we need to subtract the

leading-order constant energy dissipation from the dissipation term in the KHM equations (Lindborg 1999; Xie & Bühler 2018).

Therefore, assuming that the buoyancy potential energy transfers downscale, following the argument of 3-D turbulence, (3.2*b*) implies

$$\boldsymbol{\nabla}\cdot\overline{\delta\boldsymbol{u}\,\delta\sigma^2}=\text{constant}. \tag{3.10}$$

Similarly, as the kinetic energy transfers upscale in our 2-D system, after subtracting the leading-order energy injection by buoyancy terms and the constant energy dissipation, (3.2*a*) results in

$$-\frac{1}{2}\boldsymbol{\nabla}\cdot\overline{\delta\boldsymbol{u}(\delta u^2+\delta w^2)}+f(-\overline{\delta u\,\delta\sigma}+\overline{\delta w\,\delta\theta})=0. \tag{3.11}$$

Combining (3.10) and (3.11), and invoking the dimensional analysis, we obtain the third- and second-order structure functions

$$V_K^{(1)}\equiv\overline{\delta u(\delta u^2+\delta w^2)}\sim r^{9/5}, \tag{3.12a}$$

$$V_P^{(1)}\equiv\overline{\delta u(\delta\sigma^2+\delta\theta^2)}\sim -r, \tag{3.12b}$$

$$\overline{\delta u^2}\sim\overline{\delta w^2}\sim r^{6/5}, \tag{3.12c}$$

$$\overline{\delta\sigma^2}\sim\overline{\delta\theta^2}\sim r^{2/5}, \tag{3.12d}$$

which are exactly the predictions of the BO theory. Here, the upper index $^{(1)}$ denotes the horizontal component of the structure function vector, and correspondingly, we define $V_K^{(2)}\equiv\overline{\delta w\left(\delta u^2+\delta w^2\right)}$ and $V_P^{(2)}\equiv\overline{\delta w\left(\delta\sigma^2+\delta\theta^2\right)}$ for the vertical components. The signs of the third-order structure functions correspond to the direction of energy flux. The positive and negative signs correspond to the downscale and upscale fluxes, respectively (Cho & Lindborg 2001; Xie & Bühler 2019*a*). Note that to obtain (3.12*b*), we do not need to invoke the dimensional analysis, so it is more robust compared with other relations. Also, in above derivation we make use of the inverse cascade of kinetic energy to obtain (3.11), therefore we claim that the BO scaling coexists with the inverse kinetic energy cascade, which is supported by our numerical results shown in § 4.

The high-order structure functions may also be power functions of the two-point distance, i.e.

$$\overline{\delta u^n}\sim r^{\zeta_u}\quad\text{and}\quad\overline{\delta\theta^n}\sim r^{\zeta_\theta}, \tag{3.13a,b}$$

where ζ_u and ζ_θ are both functions of n. In a non-intermittent situation, the BO scenario implies

$$\zeta_u=\tfrac{3}{5}n\quad\text{and}\quad\zeta_\theta=\tfrac{1}{5}n. \tag{3.14a,b}$$

4. Numerical simulations

In this section, we perform numerical simulations of the isotropic convection system based on (2.5*a*)–(2.5*c*) to justify the above theoretical argument. The simulations use a Fourier pseudospectral method with 2/3 de-aliasing in space, resolutions up to 2048 × 2048, and a fourth-order explicit Runge–Kutta scheme in time, in which the nonlinear terms are treated explicitly and linear terms implicitly using an integrating factor method. Since we focus on the scales away from the impact of dissipation and diffusivity, we do not study the influence of Pr and thus take $\nu=\kappa$. Also, we take $\alpha=\mu$. In the simulations,

ν ranges from 10^{-12} to 10^{-16}, and $\alpha = 2$ is fixed. This parameter setting results in a hyperviscosity-based *Ra* range 10^{24}–10^{32}, equivalent to a range 10^6–10^8 based on the usual definition. In the simulation with resolution 2048×2048, to obtain trustable statistics, we run the simulation to a statistically steady state and maintain for 5×10^4 eddy turnover time, which is calculated as the inverse of the mean square vorticity.

To extend the inertial range, we apply hyperviscosity instead of the ordinary viscosity. The impact of hyperviscosity has been studied before; e.g. Jimenez (1994) found that hyperviscosity brings about oscillatory tails to vortices. As the order of hyperviscosity increases, the Navier–Stokes equation behaves more like the truncated Euler equation, and the energy spectrum scales as k^2 instead of the Kolmogorov scaling $k^{-5/3}$ in 3-D turbulence (Frisch *et al.* 2008; Agrawal *et al.* 2020). Despite the above-mentioned differences between ordinary and hyperviscous flows, Haugen & Brandenburg (2004) justified that in 3-D isotropic hyperviscous turbulence, particularly with the viscous operator ∇^6, scalings of structure functions up to 8th order are consistent with those obtained in ordinary viscous turbulence, therefore we use the hyperviscous operator ∇^6 in our model (2.5*a*)–(2.5*c*).

4.1. *Turbulent fields*

We first present some important features of the turbulent fields using the numerical results with $\nu = 10^{-16}$. Figure 1 shows snapshots of vorticity $\nabla^2\psi$ and two buoyancy fields. It is seen that the vertical buoyancy field θ, which contains up- and down-moving plumes, just resembles the temperature field in the 2-D homogeneous RBC system (Celani *et al.* 2000). However, it differs from the horizontal buoyancy field σ, where left- and right-moving plumes are present. Their difference can be seen from the asymmetry of sharp interfaces: in the θ field, the horizontal sharp interfaces prefer negative gradients of θ, while the vertical interfaces consist of nearly symmetric positive and negative gradient of θ; and vice versa for the σ field. Thus the combination of θ and σ leads to the present isotropic convection.

The isotropic feature of the turbulent fields is illustrated further in figure 2, where the second- and third-order isotropic fields, including $\overline{\delta u^2} + \overline{\delta w^2}$, $\overline{\delta\sigma^2} + \overline{\delta\theta^2}$, $\boldsymbol{\nabla} \cdot V_K$ and $\boldsymbol{\nabla} \cdot V_P$, are plotted separately. As expected, all these fields show isotropic behaviours, which will be confirmed quantitatively later. Although anisotropy is present at large scales, owing to the effect of the square periodic box, the flows at these scales are dominated by large-scale damping and therefore do not affect the statistics at scales where BO scaling presents.

4.2. *Low-order structure functions*

In § 3.2, we discussed that the key for the BO scenario is associated with the transfer directions of the potential and kinetic energy. Here, we present the numerical evidence. Figure 3 shows the kinetic and potential energy fluxes, and their difference is also presented because the buoyancy terms in the kinetic and potential energy equations cancel. It is seen that the potential energy transfers downscale and the kinetic energy transfers upscale, thus supporting the assumption proposed in § 3.2. And the wide plateau appearing in their difference justifies not only the negligible effects of dissipation and diffusivity, but also the correctness of our simulations. We also compare the potential energy fluxes in simulations with different ν. It is seen that decreasing the hyperviscosity results in a wider range for the approximately constant potential energy flux, and therefore

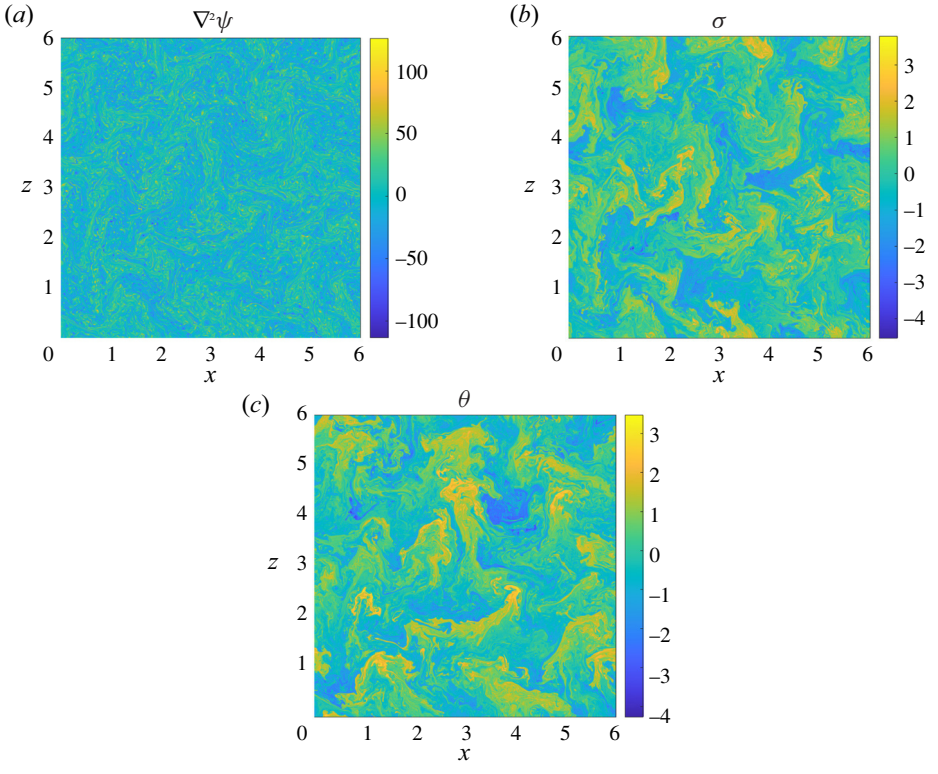

Figure 1. Snapshots of $\nabla^2\psi$, σ and θ at a statistically steady state.

extends the possible range for detecting the BO scaling. In other words, the present isotropic convection system would exhibit the BO scaling more evidently with smaller hyperviscosities (equivalently, at larger *Ra* values).

To verify the above discussion quantitatively, and most importantly the scaling relations (3.12) derived in § 3.3, we now check in figure 4 the third-order structure functions corresponding to the kinetic and potential energy fluxes. There exists a wide range of length scales in which the data closely follow the BO scaling. Moreover, the results in figure 4(*b*) show that the BO scaling range extends much further as the hyperviscosity decreases, confirming the discussion above. Here, the isotropic features of the present system are verified quantitatively by comparing the results in different directions. Similarly, the second-order structure functions shown in figure 5 also follow the BO scalings. In addition, the well-collapsed data for different directions and components further demonstrate the isotropy of the flow fields. Thus combining the information of figures 4 and 5, we can conclude safely that the BO scaling is well observed in the low-order structure functions of the present isotropic convection system.

4.3. *High-order structure functions*

In this section, we study the high-order structure functions. Because the flow fields well satisfy the isotropic condition, we focus on the statistics of the horizontal velocity u and the temperature field θ. In figure 6, we plot the structure functions of δu and $\delta\theta$ from order 2 to order 9, and the corresponding scaling exponents ζ_u and ζ_θ (cf.

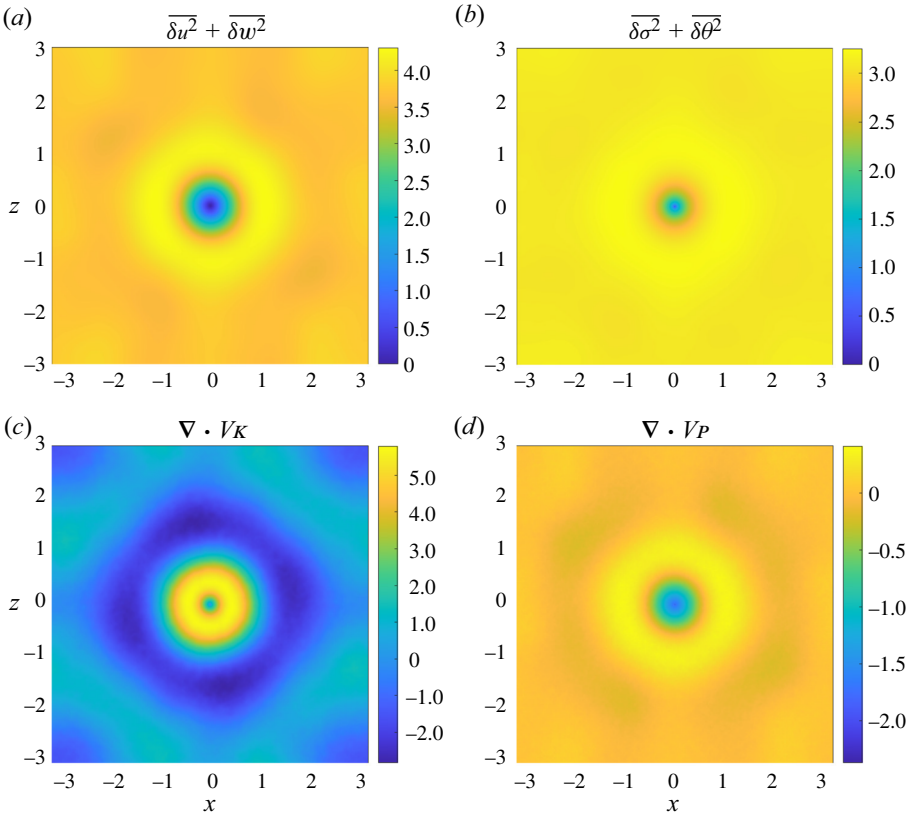

Figure 2. Isotropic fields of $\overline{\delta u^2} + \overline{\delta w^2}$, $\overline{\delta \sigma^2} + \overline{\delta \theta^2}$, $\nabla \cdot V_K$ and $\nabla \cdot V_P$.

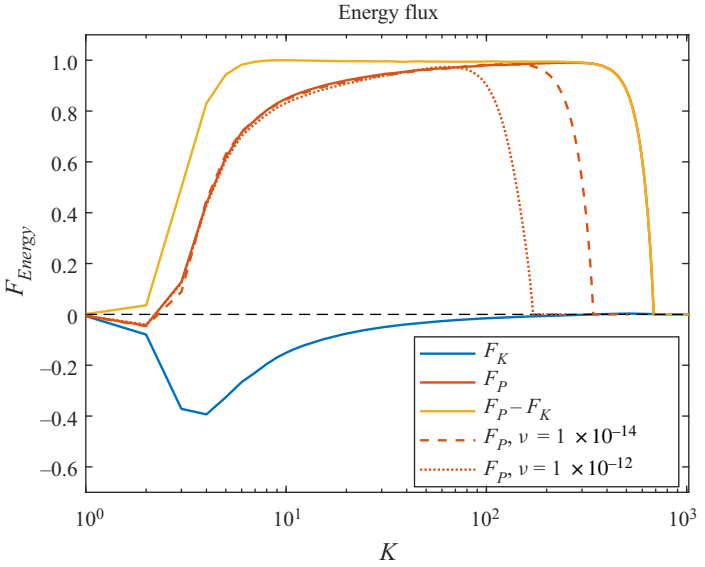

Figure 3. Kinetic (F_K) and potential (F_P) energy fluxes, as well as their difference. Potential energy fluxes with different hyperviscosities are also plotted for comparison.

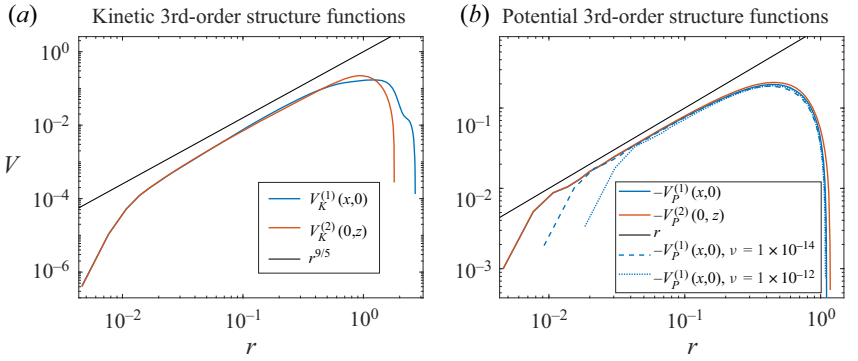

Figure 4. The third-order structure functions corresponding to the kinetic and potential energy fluxes at different directions. The BO scalings are plotted for reference. Again, the data with different hyperviscosities are plotted in panel (*b*) for comparison.

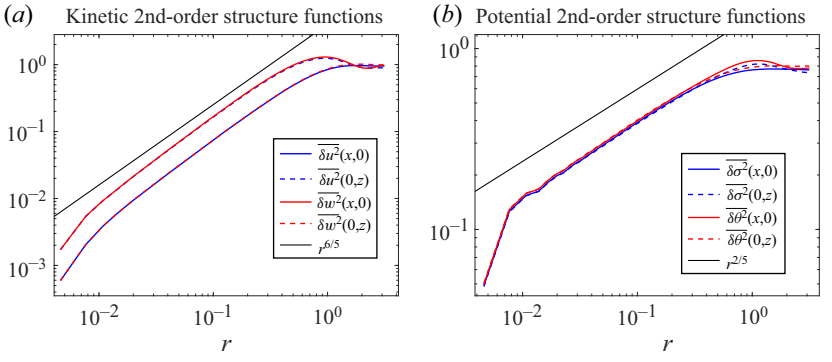

Figure 5. The second-order structure functions of (*a*) velocity and (*b*) temperature fields for different components and directions. The BO scalings are plotted for reference.

(3.13*a*,*b*)) in the inertial range are also shown. Note that only the absolute values of S_n^θ are exhibited, as the high-order structure functions of θ can be negative. Figures 6(*c*,*d*) show the compensated plots of the ninth-order structure functions of u and θ, to show the quality of scaling behaviour. The compensated scaling $r^{27.3/5}$ in the velocity structure function is very close to the BO scaling $r^{27/5}$. A bottleneck effect (cf. Frisch *et al.* 2008) is seen in the structure function of θ, but the scaling recalls similar behaviour observed in 3-D isotropic turbulence by Haugen & Brandenburg (2004). The bottleneck effect is not seen in the velocity structure function; this is because the kinetic cascades upscale while the potential energy cascades downscale. The high-order structure functions do have power-function dependence on two-point distance. The non-intermittent BO scaling $\zeta_u = 3n/5$ (cf. (3.14*a*,*b*)) well captures the behaviour of the high-order velocity structure functions, but the temperature structure functions show strong intermittency. It is seen that the scaling exponent ζ_θ deviates from the BO prediction (i.e. $\zeta_\theta = n/5$) and saturates to value 0.75 as $n \geq 5$, which is similar to the results in 2-D homogeneous RBC (Celani *et al.* 2002). However, an interesting observation is that $\overline{\delta\theta^3} \sim r^{3/5}$, which was not shown in previous studies.

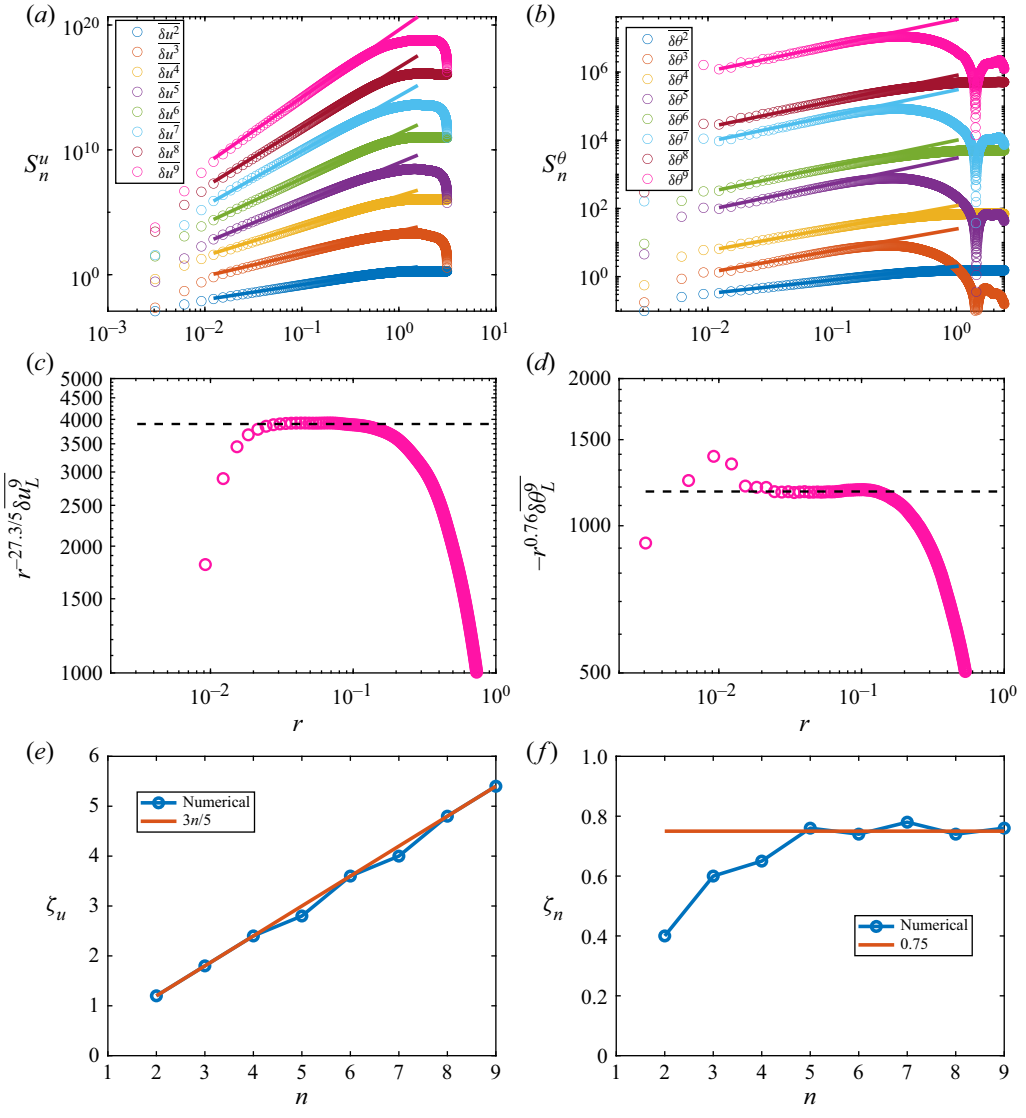

Figure 6. (*a*,*b*) Structure functions S_n^u and S_n^θ with $n = 2, 3, 4, 5, 6, 7, 8, 9$. The curves are shifted vertically. (*c*,*d*) Compensated ninth-order structure functions of u and θ, where the horizontal dashed lines are presented for reference. The power-function fittings to the data in the BO scaling range are also presented. (*e*,*f*) Corresponding scaling exponents ζ_u and ζ_θ.

The intermittent effects can be also observed in the p.d.f.s of, for example, the normalized longitudinal velocity increment δu_L and temperature increment $\delta\theta_L$, as shown in figure 7. Here, δu_L is evaluated with the x-direction displacement, and $\delta\theta_L$ is evaluated with the z-direction displacement. It is seen that the p.d.f.s of δu_L for different scales are well collapsed and all Gaussian-like, though the upscale energy transfer brings about positive skewness, which resembles that in the inverse cascade range of 2-D turbulence (cf. Boffetta, Celani & Vergassola 2000; Boffetta & Ecke 2012). However, the p.d.f.s of $\delta\theta_L$ for different scales do not fall on top of each other, and their departure from the

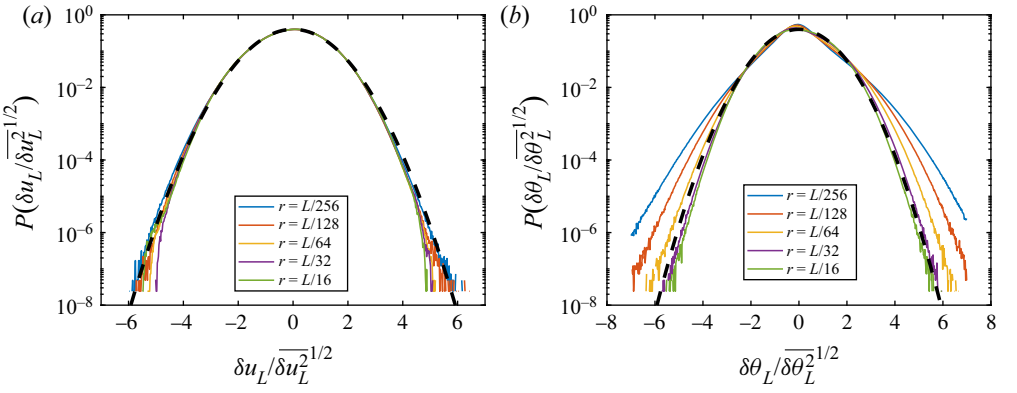

Figure 7. P.d.f.s of normalized δu_L and $\delta\theta_L$; r is the distance between two measured points. The black dashed line is the normal distribution for reference.

Gaussian distribution becomes much stronger at smaller scales, manifesting the effects of intermittency (Celani *et al.* 2001).

Figure 8 shows the integration kernels for the sixth- and eighth-order structure functions of u and θ, which justify the convergence of high-order structure functions. Figures 8(*a*,*b*) show a larger probability of the positive velocity difference, which is in consistent with the positive third-order structure function $\overline{\delta u_L^3} > 0$ corresponding to an upscale kinetic energy flux shown in figure 3. This contrasts with the integration kernels observed in 3-D RBC with a forward kinetic energy cascade (cf. Sun *et al.* 2006). The collapse of integration kernels with different displacements again shows the non-intermittency of velocity differences. The integration kernels of temperature structure functions shown in figures 8(*c*,*d*) show a preference of negative values, which is in accord with the plumes structures (cf. figure 1). The hot plumes travel upwards and cold plumes travel downwards, so collisions of plumes give strong negative and weak positive θ gradients in the vertical direction. This negative-value preference is also observed in 3-D RBC (Sun *et al.* 2006). Different from the integration kernels of velocity difference, those of temperature difference with different displacements do not collapse, indicating strong intermittency, which is consistent with figure 7(*b*).

4.4. *RBC in a periodic domain*

To gain a better understanding of the present isotropic convection system, we compare it with the homogeneous RBC system, i.e. the canonical anisotropic RBC in a periodic domain. The simulation uses the same algorithm as for the isotropic system with $\nu = 10^{-16}$, but without the horizontal component in the buoyancy field. To obtain trustable statistics, we run the simulation to a statistically steady state and maintain for 8×10^4 eddy turnover time, which is calculated as the inverse of the mean square vorticity. The convergence of the statistics has also been checked by calculating the integral kernels of structure functions (not shown here) as in figure 8.

Figure 9 shows some statistical quantities of the homogeneous RBC, which are the counterparts of those shown in figure 2. It is seen that even the second-order statistics have exhibited obvious anisotropic features, which elongate along the vertical direction as expected. When it comes to the third-order statistics, the anisotropy is more dramatic, resulting in the longitudinal and transversal structure functions being distinctive.

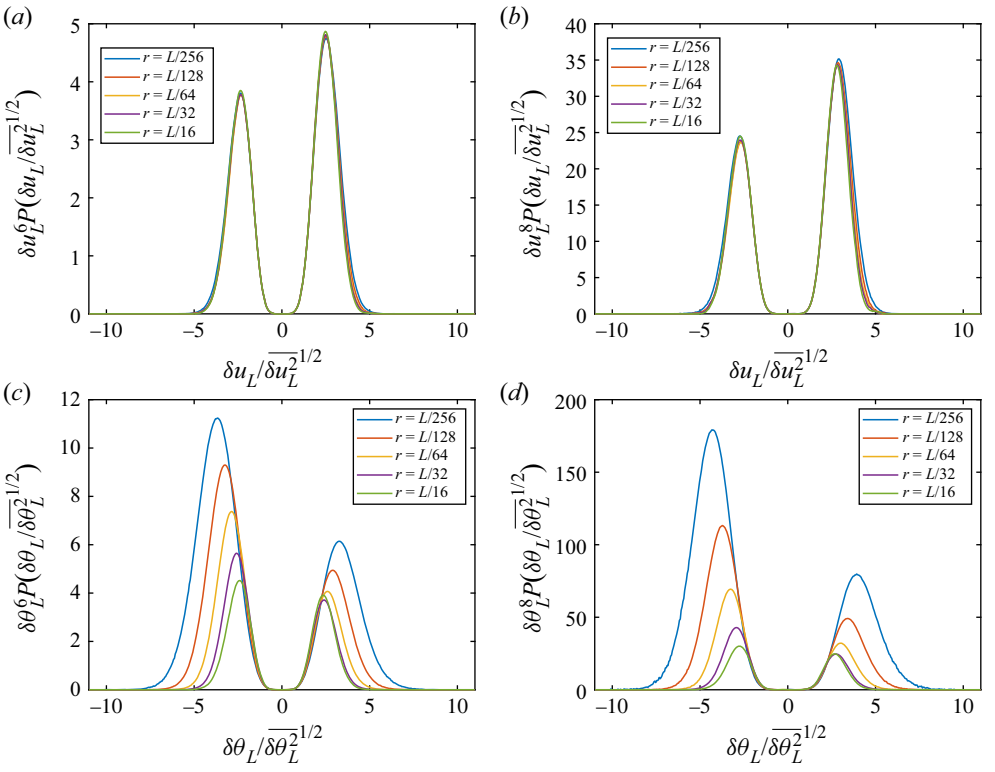

Figure 8. Integration kernels for the sixth- and eighth-order longitudinal structure functions of u and θ with different displacements of two measured points.

To further illustrate the impact of anisotropy, we show in figure 10 the third-order structure functions corresponding to kinetic and potential energy fluxes in different directions in the anisotropic RBC, which are the counterparts of those shown in figure 4. Figure 10(a) shows that both the horizontal and vertical components of the kinetic energy structure function deviate from the BO scaling, with a steeper scaling for the horizontal component and a shallower scaling for the vertical component. For the potential energy structure function, the vertical component is close to the BO scaling, while the horizontal component is shallower. The anisotropic behaviour of both the kinetic and potential energy third-order structure functions, which differ from the isotropic structure functions of our isotropic system (cf. figure 4), shows the anisotropic energy flux phenomenon in the homogeneous RBC.

The anisotropy traces back to instability, which drives the turbulent dynamics. In homogeneous RBC, the linear growth rate λ_{RBC} with respect to the zero state of (2.1a)–(2.1b) reads

$$\lambda_{RBC} = \frac{1}{2}\left(-(\nu_0+\kappa_0)K^2 + \sqrt{(\nu_0+\kappa_0)^2K^4 - 4\nu_0\kappa_0K^4 + \frac{4g\beta k^2}{K^2}}\right), \tag{4.1}$$

which is anisotropic. For horizontal modes with $\boldsymbol{k} = (0, m)$, the growth rate λ_{RBC} is negative, therefore these modes are linearly stable and do not inject energy into the system, while the most unstable mode is a so-called elevator mode with $m = 0$. Therefore, it

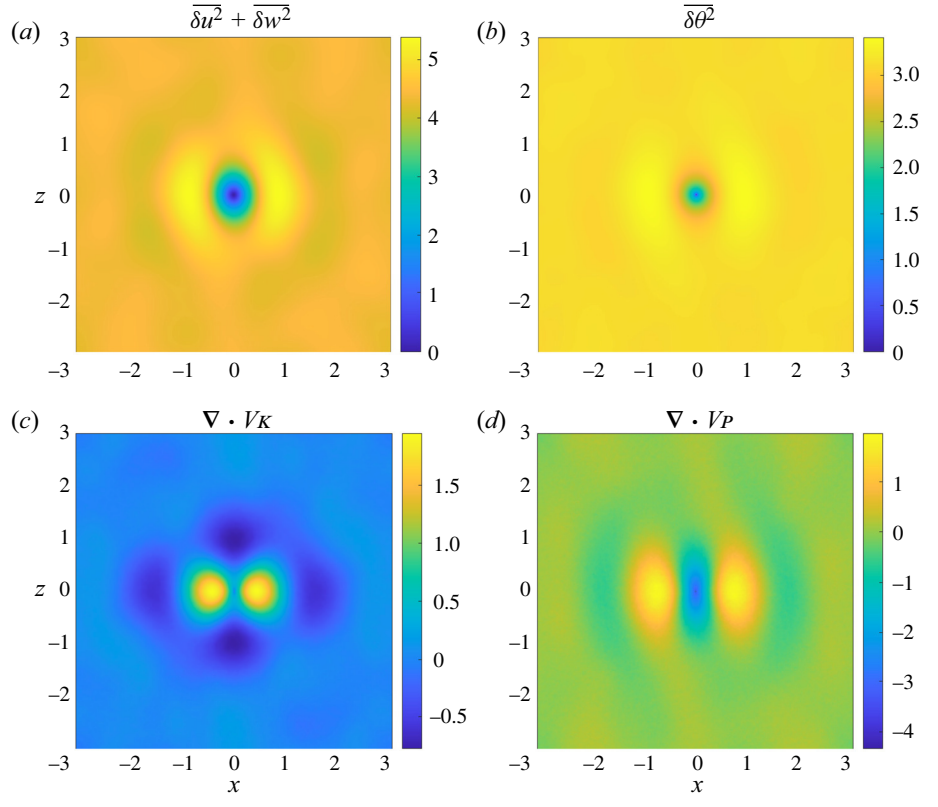

Figure 9. Isotropic fields of $\overline{\delta u^2} + \overline{\delta w^2}$, $\overline{\delta\theta^2}$, $\nabla \cdot V_K$ and $\nabla \cdot V_P$ in 2-D homogeneous (but anisotropic) RBC.

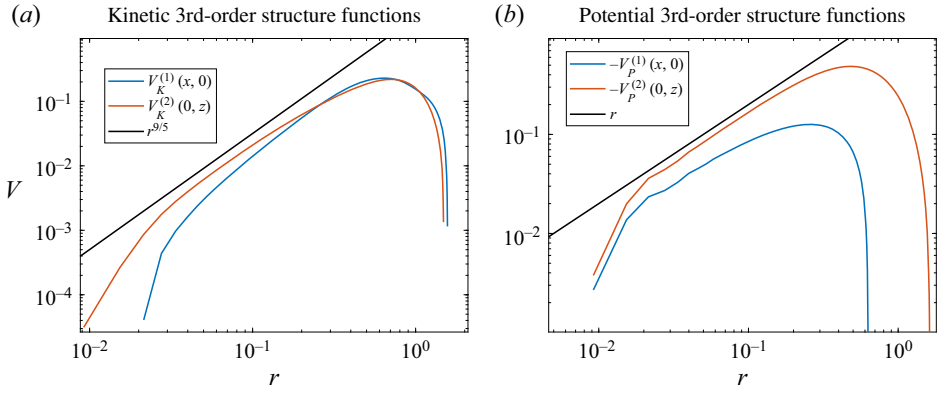

Figure 10. The third-order structure functions corresponding to the kinetic and potential energy fluxes at different directions in anisotropic RBC. The BO scalings are plotted for reference.

is expected to observe more flow structures – plumes – propagating vertically. So in figures 9(*c*,*d*), the divergence of third-order structure functions, which correspond to energy sources and sinks, concentrate around locations with zero vertical displacement. Considering that in the spectral space the nonlinear advection transfers energy from sources, where the modes are unstable, to sinks, the anisotropic growth rate (cf. (4.1))

leads to anisotropic energy transfer (cf. figure 10), which further leads to anisotropic structure functions in inertial ranges. It is this anisotropic energy transfer that contaminates the scaling behaviour in the canonical RBC. Note that an alternative way to analyse the anisotropy in turbulent flows is by examining structure functions with different symmetry (cf. Biferale & Procaccia 2005), which is beyond the scope of this paper.

5. Summary and discussion

In this paper, we construct a 2-D isotropic convection system in a doubly periodic domain, aiming to explore the BO scaling in a situation without any complicating factor that contaminates the scaling properties. The periodic domain avoids the impact of the walls and the large-scale circulations, and the 2-D formulation with upscale kinetic energy flux enables the observation of a long inertial range for the BO scenario. These advantages are shared with previous studies of 2-D homogeneous RBC (Biskamp & Schwarz 1997; Biskamp *et al.* 2001; Celani *et al.* 2001; Mazzino 2017) and RT turbulence (Chertkov 2003; Boffetta *et al.* 2012). However, the turbulent fields in those systems are still anisotropic, making the scaling properties of structure functions depend on the evaluated direction, as we demonstrated in § 4.4. By introducing an extra buoyancy field subjected to horizontal gravity, we successfully obtain an isotropic convection system, which makes the structure functions directional-independent, and thus it is perfect to explore the BO scenario.

Based on the downscale flux of the potential energy and the upscale flux of the kinetic energy, we derive structure function relations from the KHM equations for the present isotropic convection system. And invoking self-similarity, these structure function relations lead directly to the BO scaling, which is checked with direct numerical simulations. It is found that the second- and third-order structure functions of velocity and buoyancy all follow the BO scaling. For high-order structure functions, the velocity field shows no intermittency, but the buoyancy field shows strong intermittency with the scaling exponent $\zeta_\theta \to 0.75$ as the order $n \geq 5$. These results for high-order structure functions are similar to those observed in 2-D homogeneous RBC (Celani *et al.* 2002; Mazzino 2017), while in 2-D RBC, ζ_θ tends to a value ($\sim$0.8) slightly larger than 0.75. The major difference is that the third-order structure function of buoyancy in the isotropic convection follows the BO scaling perfectly, contradicting the result in homogeneous RBC. We believe that this difference stems from the isotropy as discussed in § 4.4.

We end this paper by noting the key for detecting the BO scaling, which has been conjectured to be associated with the inverse kinetic energy cascade (Boffetta *et al.* 2012). Although some RBC experiments on soap films/bubbles have reported BO-like scaling, the direction of the kinetic energy flux in these studies was unclear (Zhang & Wu 2005; Seychelles *et al.* 2010). Thus our theoretical argument and numerical results provide direct support for the validity of this conjecture in RBC. While the present 2-D isotropic convection is physically unrealizable, the realization of inverse kinetic energy cascade in a laboratory is quite feasible. One promising approach is to use geometrical confinement, i.e. a quasi-2-D system, as Boffetta *et al.* (2012) did in the study of RT turbulence. Some recent studies of quasi-2-D RBC have observed the condensation of turbulent structures (Huang *et al.* 2013; Chong *et al.* 2015), which is an intriguing feature due to the inverse kinetic energy cascade (Xia *et al.* 2011). In this context, the present 2-D system is also worthwhile to extend to its counterparts in quasi-2-D and 3-D systems, which may help to reveal the connection between 2-D and 3-D RBC in terms of small-scale statistics. We expect that the present 2-D isotropic convection can not only improve theoretical understanding of canonical RBC, but also stimulate experiments that go beyond the canonical RBC

configuration, which is exactly the current trend in the field of turbulent convection (Xia 2013).

Acknowledgement. The authors thank K.-Q. Xia for helpful discussions.

Funding. J.-H.X. gratefully acknowledges financial support from the National Natural Science Foundation of China (NSFC) under grant no. 92052102, and the Joint Laboratory of Marine Hydrodynamics and Ocean Engineering, Pilot National Laboratory for Marine Science and Technology (Qingdao). S.-D.H. is supported by the NSFC (grant nos 11988102, 11961160719 and 91752201) and the Department of Science and Technology of Guangdong Province (grant no. 2019B21203001).

Declaration of interests. The authors report no conflict of interest.

Author ORCIDs.
Jin-Han Xie https://orcid.org/0000-0003-0502-8662;
Shi-Di Huang https://orcid.org/0000-0001-5719-6428.

Appendix A. Statistics of some other isotropic quantities

In this appendix, we study the structure functions of some isotropic scalars that are non-intermittent. Due to the presence of a horizontal buoyancy field, we can introduce two isotropic scalar quantities, namely Ψ and Φ, through the Helmholtz decomposition of buoyancy fields, as

$$(\sigma, \theta) = \boldsymbol{\nabla}\Phi + \boldsymbol{\nabla}^{\perp}\Psi. \tag{A1}$$

It is natural to study their structure functions together with the streamfunction ψ. Based on the discussion in § 3, a simple dimensional analysis implies that

$$\delta\psi \sim r^{8/5} \quad \text{and} \quad \delta\Phi \sim \delta\Psi \sim r^{6/5}, \tag{A2a,b}$$

which, however, is problematic. This is because, for the second-order statistics, we have

$$\nabla^2\overline{\delta\psi^2} = 2(\overline{u^2} + \overline{w^2} - \overline{\delta u^2} - \overline{\delta w^2}). \tag{A3}$$

As $\overline{\delta u^2} + \overline{\delta w^2} \sim r^{6/5}$ follows the BO scaling, we immediately obtain

$$\overline{\delta\psi^2} \sim r^2 + \text{h.o.t.} \tag{A4}$$

when considering the small-r limit, which is in contrast to (A2*a*,*b*). Note that (A4) holds as long as the scaling exponent of $\overline{\delta u^2} + \overline{\delta w^2}$ is positive. However, the high-order structure functions of $\delta\psi$ do not have relations like (A3) that are linked to the structure functions of δu, so their scalings are unknown. Nevertheless, according to (A4), a naive guess for the nth-order structure functions of $\delta\psi$ (without intermittency) is

$$\overline{\delta\psi^n} \sim r^n. \tag{A5}$$

Similarly, the structure functions of $\delta\Psi$ and $\delta\Phi$ for the leading order are expected to be

$$\overline{\delta\Psi^n} \sim r^n \quad \text{and} \quad \overline{\delta\Phi^n} \sim r^n. \tag{A6a,b}$$

Now we use the numerical data to check the scaling relations (A5) and (A6*a*,*b*). In figure 11, we show the structure functions of ψ, Ψ and Φ for different orders, together with their scaling exponents obtained in the inertial range. For the structure functions of ψ and Ψ, we plot their absolute values, but for the structure functions of Φ, we plot the positive and negative parts separately due to their different scaling behaviours. It is seen that all the

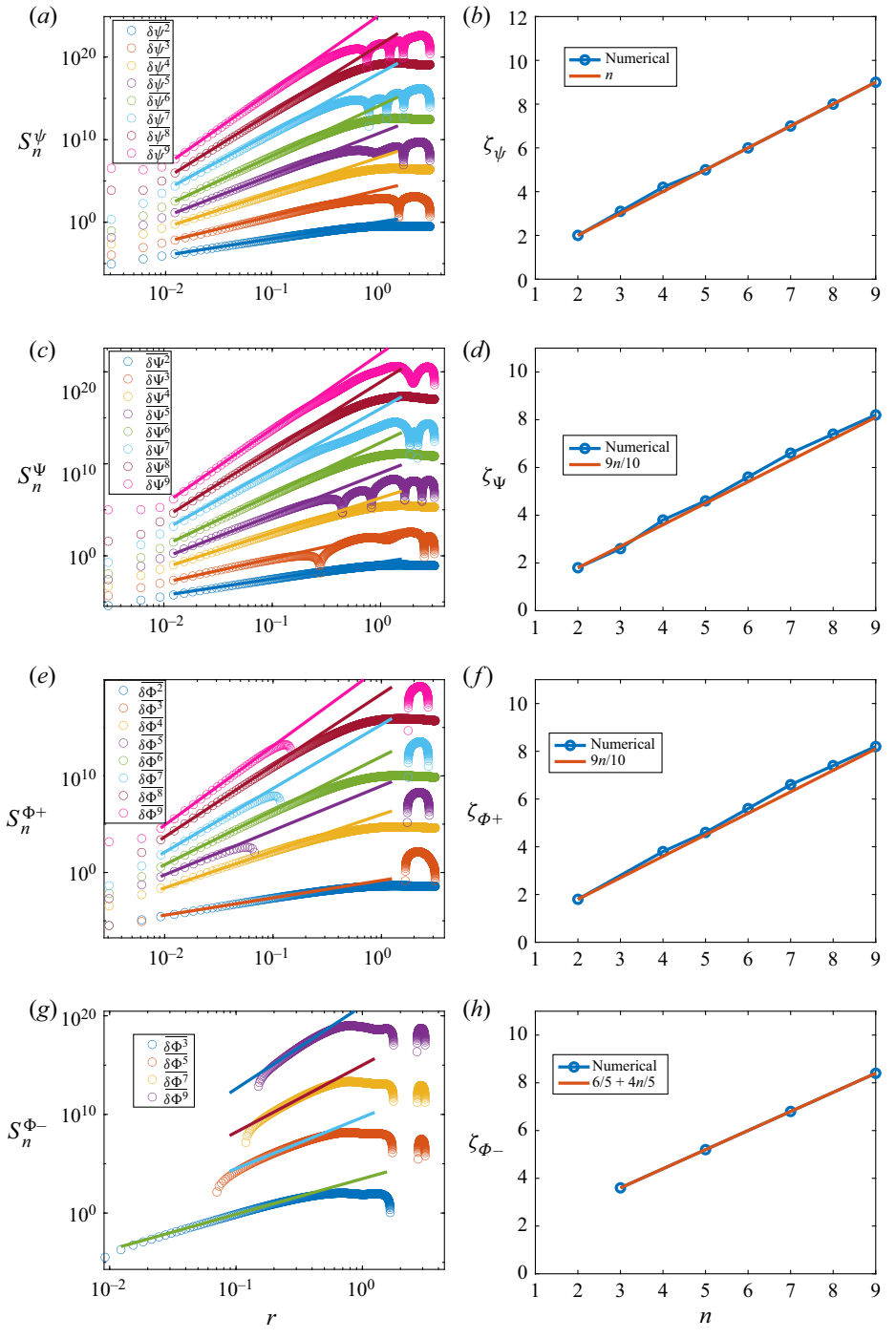

Figure 11. Structure functions of (a,c,e,g) ψ, Ψ and Φ and (b,d,f,h) their scalings. The absolute values of structure functions of ψ and Ψ are presented as S_n^{ψ} and S_n^{Ψ}, respectively. Here, $S_n^{\Phi+}$ and $S_n^{\Phi-}$ denote the positive and negative parts of the structure functions of Φ.

structure functions exhibit power-function dependencies and no intermittency is observed, but their scaling exponents are distinctive. To be specific, while the scaling exponents ζ_ψ of the structure functions of ψ follow (A5) nicely, those for the structure functions of Ψ show a non-expected dependence as $\zeta_\Psi = 9n/10$. Note that even for $n = 2$, ζ_Ψ differs from the prediction given by (A6*a*,*b*), though their differences are not that much. More interestingly, the positive and negative parts of the structure functions of Φ exhibit different scalings. While the scalings for the positive part also follow a dependence as $\zeta_{\Phi+} = 9n/10$, those for the negative part have a more strange behaviour as $\zeta_{\Phi-} = 6/5 + 4n/5$. We do not have an explanation for the behaviour of these scaling exponents, which is subject to future study.

References

Agrawal, R., Alexakis, A., Brachet, M.E. & Tuckerman, L.S. 2020 Turbulent cascade, bottleneck, and thermalized spectrum in hyperviscous flows. *Phys. Rev. Fluids* **5**, 024601.

Ahlers, G., Grossmann, S. & Lohse, D. 2009 Heat transfer and large scale dynamics in turbulent Rayleigh–Bénard convection. *Rev. Mod. Phys.* **81**, 503–537.

Benzi, R., Ciliberto, S., Tripiccione, R., Baudet, C., Massaioli, F. & Succi, S. 1993 Extended self-similarity in turbulent flows. *Phys. Rev.* E **48** (1), R29–R32.

Biferale, L., Calzavarini, E., Toschi, F. & Tripiccione, R. 2003 Universality of anisotropic fluctuations from numerical simulations of turbulent flows. *Europhys. Lett.* **64** (4), 461–467.

Biferale, L. & Procaccia, I. 2005 Anisotropy in turbulent flows and in turbulent transport. *Phys. Rep.* **414**, 43–164.

Biskamp, D., Hallatschek, K. & Schwarz, E. 2001 Scaling laws in two-dimensional turbulent convection. *Phys. Rev.* E **63**, 045302(R).

Biskamp, D. & Schwarz, E. 1997 Scaling properties of turbulent convection in two-dimensional periodic systems. *Europhys. Lett.* **40** (6), 637–642.

Boffetta, G., Celani, A. & Vergassola, M. 2000 Inverse energy cascade in two-dimensional turbulence: deviations from Gaussian behavior. *Phys. Rev.* E **61** (1), R29.

Boffetta, G., De Lillo, F., Mazzino, A. & Musacchio, S. 2012 Bolgiano scale in confined Rayleigh–Taylor turbulence. *J. Fluid Mech.* **690**, 426–440.

Boffetta, G. & Ecke, R.E. 2012 Two-dimensional turbulence. *Annu. Rev. Fluid Mech.* **44**, 427–451.

Boffetta, G. & Mazzino, A. 2017 Incompressible Rayleigh–Taylor turbulence. *Annu. Rev. Fluid Mech.* **49**, 119–143.

Boffetta, G., Mazzino, A., Musacchio, S. & Vozella, L. 2009 Kolmogorov scaling and intermittency in Rayleigh–Taylor turbulence. *Phys. Rev.* E **79**, 065301.

Bolgiano, R. 1959 Turbulent spectra in a stably stratified atmosphere. *J. Geophys. Res.* **64**, 2226–2229.

Borue, V. & Orszag, S.A. 1997 Turbulent convection driven by a constant temperature gradient. *J. Sci. Comput.* **12** (3), 305–351.

Calzavarini, E., Doering, C.R., Gibbon, J.D., Lohse, D., Tanabe, A. & Toschi, F. 2006 Exponentially growing solutions in homogeneous Rayleigh–Bénard convection. *Phys. Rev.* E **73**, 0345301(R).

Calzavarini, E., Toschi, F. & Tripiccione, R. 2002 Evidences of Bolgiano–Obhukhov scaling in three-dimensional Rayleigh–Bénard convection. *Phys. Rev.* E **66**, 016304.

Camussi, R. & Verzicco, R. 2004 Temporal statistics in high Rayleigh number convective turbulence. *Eur. J. Mech. B/Fluids* **23**, 427–442.

Celani, A., Lanotte, A., Mazzino, A. & Vergassola, M. 2000 Universality and saturation of intermittency in passive scalar turbulence. *Phys. Rev. Lett.* **84**, 2385–2388.

Celani, A., Matsumoto, T., Mazzino, A. & Vergassola, M. 2002 Scaling and universality in turbulent convection. *Phys. Rev. Lett.* **88**, 054503.

Celani, A., Mazzino, A. & Vergassola, M. 2001 Thermal plume turbulence. *Phys. Fluids* **212**, 2133–2135.

Celani, A., Mazzino, A. & Vozella, L. 2006 Rayleigh–Taylor turbulence in two dimensions. *Phys. Rev. Lett.* **96**, 134504.

Chertkov, M. 2003 Phenomenology of Rayleigh–Taylor turbulence. *Phys. Res. Lett.* **91** (11), 115001.

Chillà, F. & Schumacher, J. 2012 New perspectives in turbulent Rayleigh–Bénard convection. *Eur. Phys. J.* E **35**, 58.

CHING, E.S.C. 2007 Scaling laws in the central region of confined turbulent thermal convection. *Phys. Rev.* E **75**, 056302.

CHING, E.S.C. 2014 *Statistics and Scaling in Turbulent Rayleigh–Bénard Convection*. Springer.

CHING, E.S.C., TSANG, Y.-K., FOK, T.N., HE, X. & TONG, P. 2013 Scaling behavior in turbulent Rayleigh–Bénard convection revealed by conditional structure functions. *Phys. Rev.* E **87**, 013005.

CHO, J.Y.N. & LINDBORG, E. 2001 Horizontal velocity structure functions in the upper troposphere and lower stratosphere 1. Observations. *J. Geophys. Res.* **106** (D10), 10223–10232.

CHONG, K.L., HUANG, S.-D., KACZOROWSKI, M. & XIA, K.-Q. 2015 Condensation of coherent structures in turbulent flows. *Phys. Rev. Lett.* **115**, 264503.

CORRSIN, S. 1951 On the spectrum of isotropic temperature fluctuations in isotropic turbulence. *J. Appl. Phys.* **22**, 469–473.

FRISCH, U. 1995 *Turbulence: The Legacy of A.N. Kolmogorov*. Cambridge University Press.

FRISCH, U., KURIEN, S., PANDIT, R., PAULS, W., RAY, S.S., WIRTH, A. & ZHU, J.-Z. 2008 Hyperviscosity, Galerkin truncation, and bottlenecks in turbulence. *Phys. Rev. Lett.* **101**, 144501.

GROSSMANN, S. & LOHSE, D. 1991 Fourier–Weierstrass mode analysis for thermally driven turbulence. *Phys. Rev. Lett.* **67**, 445–448.

GROSSMANN, S. & LOHSE, D. 1992 Scaling in hard turbulent Rayleigh–Bénard flow. *Phys. Rev.* A **46**, 903–917.

HAUGEN, N.E.L. & BRANDENBURG, A. 2004 Inertial range scaling in numerical turbulence with hyperviscosity. *Phys. Rev.* E **70**, 026405.

HUANG, S.-D., KACZOROWSKI, M., NI, R. & XIA, K.-Q. 2013 Confinement-induced heat-transport enhancement in turbulent thermal convection. *Phys. Rev. Lett.* **111**, 104501.

JIMENEZ, J. 1994 Hyperviscous vortices. *J. Fluid Mech.* **279**, 169–176.

KACZOROWSKI, M., CHONG, K.-L. & XIA, K.-Q. 2014 Turbulent flow in the bulk of Rayleigh–Bénard convection: aspect-ratio dependence of the small-scale properties. *J. Fluid Mech.* **747**, 73–102.

KACZOROWSKI, M. & XIA, K.-Q. 2013 Turbulent flow in the bulk of Rayleigh–Bénard convection: small-scale properties in a cubic cell. *J. Fluid Mech.* **722**, 596–617.

KOLMOGOROV, A.N. 1941 Dissipation of energy in locally isotropic turbulence. *Dokl. Akad. Nauk SSSR* **32**, 16–18.

KRAICHNAN, R.H. 1967 Inertial ranges in two-dimensional turbulence. *Phys. Fluids* **10**, 1417.

KUNNEN, R.P.J. & CLERCX, H.J.H. 2014 Probing the energy cascade of convective turbulence. *Phys. Rev.* E **90**, 063018.

KUNNEN, R.P.J., CLERCX, H.J.H., GEURTS, B.J., VAN BOKHOVEN, L.J.A., AKKERMANS, R.A.D. & VERZICCO, R. 2008 Numerical and experimental investigation of structure-function scaling in turbulent Rayleigh–Bénard convection. *Phys. Rev.* E **77**, 016302.

LI, X.-M., HE, J.-D., TIAN, Y., HAO, P. & HUANG, S.-D. 2021*a* Effects of Prandtl number in quasi-two-dimensional Rayleigh–Bénard convection. *J. Fluid Mech.* **915**, A60.

LI, X.-M., HUANG, S.-D., NI, R. & XIA, K.-Q. 2021*b* Lagrangian velocity and acceleration measurements in plume-rich regions of turbulent Rayleigh–Bénard convection. *Phys. Rev. Fluids* **6**, 053503.

LINDBORG, E. 1999 Can the atmospheric kinetic energy spectrum be explained by two-dimensional turbulence? *J. Fluid Mech.* **388**, 259–288.

LOHSE, D. & TOSCHI, F. 2003 Ultimate state of thermal convection. *Phys. Rev. Lett.* **90** (3), 034502.

LOHSE, D. & XIA, K.-Q. 2010 Small-scale properties of turbulent Rayleigh–Bénard convection. *Annu. Rev. Fluid Mech.* **42**, 335–364.

L'VOV, V.S. 1991 Spectra of velocity and temperature fluctuations with constant entropy flux of fully developed free-convective turbulence. *Phys. Rev. Lett.* **67**, 687–690.

MASHIKO, T., TSUJI, Y., MIZUNO, T. & SANO, M. 2004 Instantaneous measurement of velocity fields in developed thermal turbulence in mercury. *Phys. Rev.* E **69**, 036306.

MAZZINO, A. 2017 Two-dimensional turbulent convection. *Phys. Fluids* **29**, 111102.

MONIN, A.S. & YAGLOM, A.M. 1975 *Statistical Fluid Mechanics, Volume II: Mechanics of Turbulence*. Dover (reprinted 2007).

NI, R., HUANG, S.-D. & XIA, K.-Q. 2011 Local energy dissipation rate balances local heat flux in the center of turbulent thermal convection. *Phys. Rev. Lett.* **107**, 174503.

OBUKHOV, A.M. 1949 Structure of the temperature field in turbulent flows. *Izv. Akad. Nauk SSSR Geogr. Geofiz* **13**, 58–69.

OBUKHOV, A.M. 1959 On influence of buoyancy forces on the structure of temperature field in a turbulent flow. *Dokl. Akad. Nauk SSSR* **125**, 1246–1248.

SEYCHELLES, F., AMAROUCHENE, Y., BESSAFI, M. & KELLAY, H. 2008 Thermal convection and emergence of isolated vortices in soap bubbles. *Phys. Rev. Lett.* **100**, 144501.

SEYCHELLES, F., INGREMEAU, F., PRADERE, C. & KELLAY, H. 2010 From intermittent to nonintermittent behavior in two dimensional thermal convection in a soap bubble. *Phys. Rev. Lett.* **105**, 264502.

SUN, C., ZHOU, Q. & XIA, K.-Q. 2006 Cascades of velocity and temperature fluctuations in buoyancy-driven thermal turbulence. *Phys. Rev. Lett.* **97**, 144504.

VERMA, M.K., KUMAR, A. & PANDEY, A. 2017 Phenomenology of buoyancy-driven turbulence: recent results. *New J. Phys.* **19**, 025012.

WU, X.-Z., KADANOFF, L., LIBCHABER, A. & SANO, M. 1990 Frequency power spectrum of temperature fluctuations in free convection. *Phys. Rev. Lett.* **64**, 2140–2143.

XIA, K.-Q. 2013 Current trends and future directions in turbulent thermal convection. *Theor. Appl. Mech. Lett.* **3**, 052001.

XIA, H., BYRNE, D., FALKOVICH, G. & SHATS, M. 2011 Upscale energy transfer in thick turbulent fluid layers. *Nat. Phys.* **7**, 321–324.

XIE, J.-H. & BÜHLER, O. 2018 Exact third-order structure functions for two-dimensional turbulence. *J. Fluid Mech.* **851**, 672–686.

XIE, J.-H. & BÜHLER, O. 2019*a* Third-order structure functions for isotropic turbulence with bidirectional energy transfer. *J. Fluid Mech.* **877**, R3.

XIE, J.-H. & BÜHLER, O. 2019*b* Two-dimensional isotropic inertia–gravity wave turbulence. *J. Fluid Mech.* **872**, 752–783.

YAKHOT, V. 1992 4/5 Kolmogorov law for statistically stationary turbulence: application to high-Rayleigh-number Bénard convection. *Phys. Rev. Lett.* **69**, 769–771.

ZHANG, J. & WU, X.L. 2005 Velocity intermittency in a buoyancy subrange in a two-dimensional soap film convection experiment. *Phys. Rev. Lett.* **94**, 234501.

ZHANG, J., WU, X.L. & XIA, K.-Q. 2005 Density fluctuations in strongly stratified two-dimensional turbulence. *Phys. Rev. Lett.* **94**, 174503.

ZHOU, Q. 2013 Temporal evolution and scaling of mixing in two-dimensional Rayleigh–Taylor turbulence. *Phys. Fluids* **25**, 085107.

ZHOU, Y. 2017 Rayleigh–Taylor and Richtmyer–Meshkov instability induced flow, turbulence, and mixing. I. *Phys. Rep.* **720–722**, 1–136.

ZHOU, Q., SUN, C. & XIA, K.-Q. 2008 Experimental investigation of homogeneity, isotropy, and circulation of the velocity field in buoyancy-driven turbulence. *J. Fluid Mech.* **598**, 361–372.